THE ASTROPHYSICAL JOURNAL, 376:245–255, 1991 July 20

THE X-RAY PROPERTIES OF GX 301−2 (4U 1223−62)

F. HABERL[1]
EXOSAT Observatory, Space Science Department of ESA, ESTEC, Noordwijk, The Netherlands
Received 1990 September 19; accepted 1991 January 21

ABSTRACT

The X-ray binary pulsar GX 301−2 (4U 1223−62/Wray 977) has been observed with *EXOSAT* at various orbital phases. As reported in the past, the X-ray luminosity shows a strong maximum near periastron passage of the neutron star (phase 0), but with the peak 0.05 in phase before. The X-ray photoelectric absorption after periastron of around 10^{24} H cm^{-2} decreases after phase 0.25 to a minimum of 1.2×10^{22} H cm^{-2} near phase 0.7. A maximum in the absorption with values up to 3×10^{24} H cm^{-2} is seen at the same orbital phase as the maximum in X-ray luminosity. During the interval between phase 0.9 and 0.25, when the absorption was high, the X-ray spectra show a strong low-energy excess which can be modeled by X-ray emission scattered around a region of enhanced wind density by the less dense ambient wind. No pulsations in the low-energy excess confirm this. Following Stevens, a model of enhanced mass loss from the primary towards the neutron star forming a dense gas stream is presented, which can reproduce the orbital phase dependence of the X-ray luminosity and absorption. In this model the strong outburst is caused by the neutron star passing through the dense gas stream before periastron. A second pass through the gas stream near phase 0.3 causes another broader increase in X-ray luminosity and leads to two minima in the light curve of GX 301−2 near phase 0.15 and 0.7. On top of the smooth phase dependence, X-ray luminosity and absorption show strong variations on time scales of hours especially during X-ray outburst.

Subject headings: pulsars — stars: accretion — stars: individual (GX 301−2) — stars: neutron — X-rays: binaries — X-rays: spectra

1. INTRODUCTION

The spectral analysis of *EXOSAT* data from 4U 1700−37 (Haberl, White, & Kallman 1989, hereafter HWK) and Vela X-1 (Haberl & White 1990, hereafter HW) has shown that a dense gas stream in the stellar wind from the primary can explain the X-ray properties of these two supergiant X-ray binaries (SXRBs). The X-ray spectra from both systems show enhanced photoelectric absorption after superior conjunction of the X-ray source caused by the dense gas stream trailing the X-ray source. A soft excess seen in the spectra below about 4 keV is caused by X-rays scattered around the gas stream by the less absorbing ambient wind. The model of scattered X-rays is confirmed by the nonpulsating nature of the low-energy excess in the Vela X-1 spectra.

Another SXRB is the 700 s X-ray pulsar GX 301−2 (4U 1223−62) with the primary Wray 977, a star of spectral type B1.5 Ia (Bradt et al. 1977). The system with an orbital period of 41.5 days (Sato et al. 1986) has the most eccentric orbit ($e = 0.47$) among the binary X-ray pulsars with well established orbital parameters (see, e.g., Joss & Rappaport 1984). The lack of an X-ray eclipse combined with a radius of the primary of 43 $R_\odot$ (Parkes et al. 1980) restricts the inclination to less than $\sim 78°$ and the mass function 33 ± 5 limits the inclination to greater than 68°, for a primary mass between 25 and 35 $M_\odot$ (Parkes et al. 1980) and a 1.4 $M_\odot$ neutron star.

The system shows strong X-ray outbursts with a period consistent with the orbital period. These outbursts last for about 5 days and are centered several days before periastron passage (Watson, Warwick, & Corbet 1982). Although simple stellar wind models can somewhat reproduce the binary phase dependence of the overall X-ray flux (White & Swank 1984), they have failed to explain this phase shift. These models predict the peak in the X-ray flux near periastron passage where the neutron star comes closest to the primary and the wind is densest along the eccentric orbit. However the asymmetry of the wind velocity relative to the neutron star causes the peak after periastron. To produce a peak in the light curve before periastron passage these models would need an implausible high mass-loss rate (Watson et al. 1982). Stevens (1988) found that the dynamical effects of the neutron star on the stellar wind can highly increase the mass-loss rate of the primary towards the neutron star near periastron in eccentric systems and might account for the strong outburst of GX 301−2.

The X-ray spectra of GX 301−2 show variable photoelectric absorption with column densities up to 2×10^{24} H cm^{-2}. The absorption seems to be highest around periastron passage (phase 0) and then decline to a minimum around phase 0.7 (White & Swank 1984). X-ray intensity dips as observed by Leahy et al. (1988) might be associated with more sudden changes in absorption. A similar behavior has been reported from Vela X-1 by HW where erratic variations in column density occurred on top of a base level of absorption. The X-ray spectra of GX 301−2 also show the presence of a soft component with much lower absorption, but it is not clear whether this is contamination from the nearby source α Cru or it has the same origin as in the spectra of 4U 1700−37 and Vela X-1.

In the light of the *EXOSAT* results from 4U 1700−37 and Vela X-1 the SXRB GX 301−2 has been investigated to search for similar X-ray properties. The *EXOSAT* observations of GX 301−2, made between 1983 August and 1985 March are summarized in § 2. The spectral analysis is presented in § 3, and in § 4 the energy dependence of the X-ray pulsations are investigated. In § 5 a model is developed to account for the

[1] Postal address: *EXOSAT* Observatory, Astrophysics Division, Space Science Department, ESTEC, Postbus 299, 220 AG Noordwijk, The Netherlands.

TABLE 1

THE *EXOSAT* OBSERVATIONS OF GX 301−2 (4U 1223−62)

DATE	TIME (UT)	ORBITAL PHASE	SPECTRAL MODE	
			N	t^a
1983 Aug 19/20	22:19–5:39	0.989–0.997	128	10
1984 Apr 20/21	22:46–6:49	0.892–0.900	128	10
1984 Apr 22	19:51–22:36	0.937–0.940	128	10
1984 Apr 24/25	21:00–0:27	0.987–0.990	128	10
1984 Jun 1	20:59–23:37	0.902–0.905	128	10
1984 Jun 4	12:16–15:55	0.966–0.969	128	10
1984 Jun 7	20:20–22:40	0.046–0.048	128	10
1984 Jun 9	5:25–8:25	0.079–0.082	128	10
1985 Feb 7/8	17:46–20:05	0.946–0.972	64	1
1985 Feb 16	0:05–13:49	0.145–0.159	64	1
1985 Feb 19/20	17:02–18:16	0.234–0.260	128	10
1985 Feb 27/28/Mar 1	3:16–1:51	0.413–0.460	64	1
1985 Mar 11	2:00–15:56	0.701–0.715	64	1

[a] The spectra obtained by the ME are binned into N channels with a time resolution given by t in s.

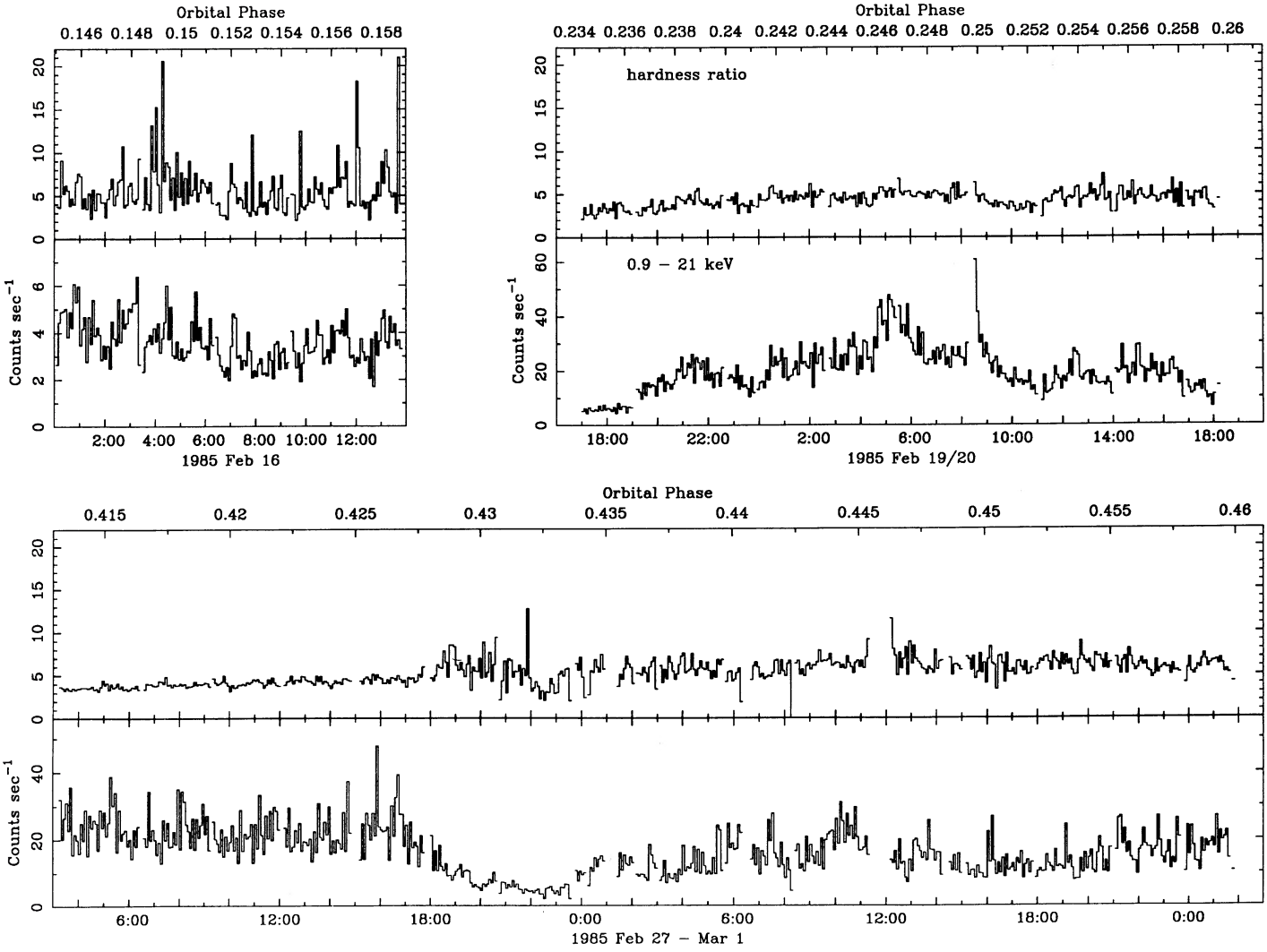

FIG. 1.—Background-subtracted light curves of GX 301−2 from the three sets of *EXOSAT* observations made in 1984 and 1985 in the energy band 0.9–21 keV and the hardness ratio of the count rates in the 4.9–21 keV and 0.9–4.9 keV bands. The count rate is in units of counts per second per half detector array with a time resolution of 300 s. For an overview of all the *EXOSAT* observations, see Table 1.

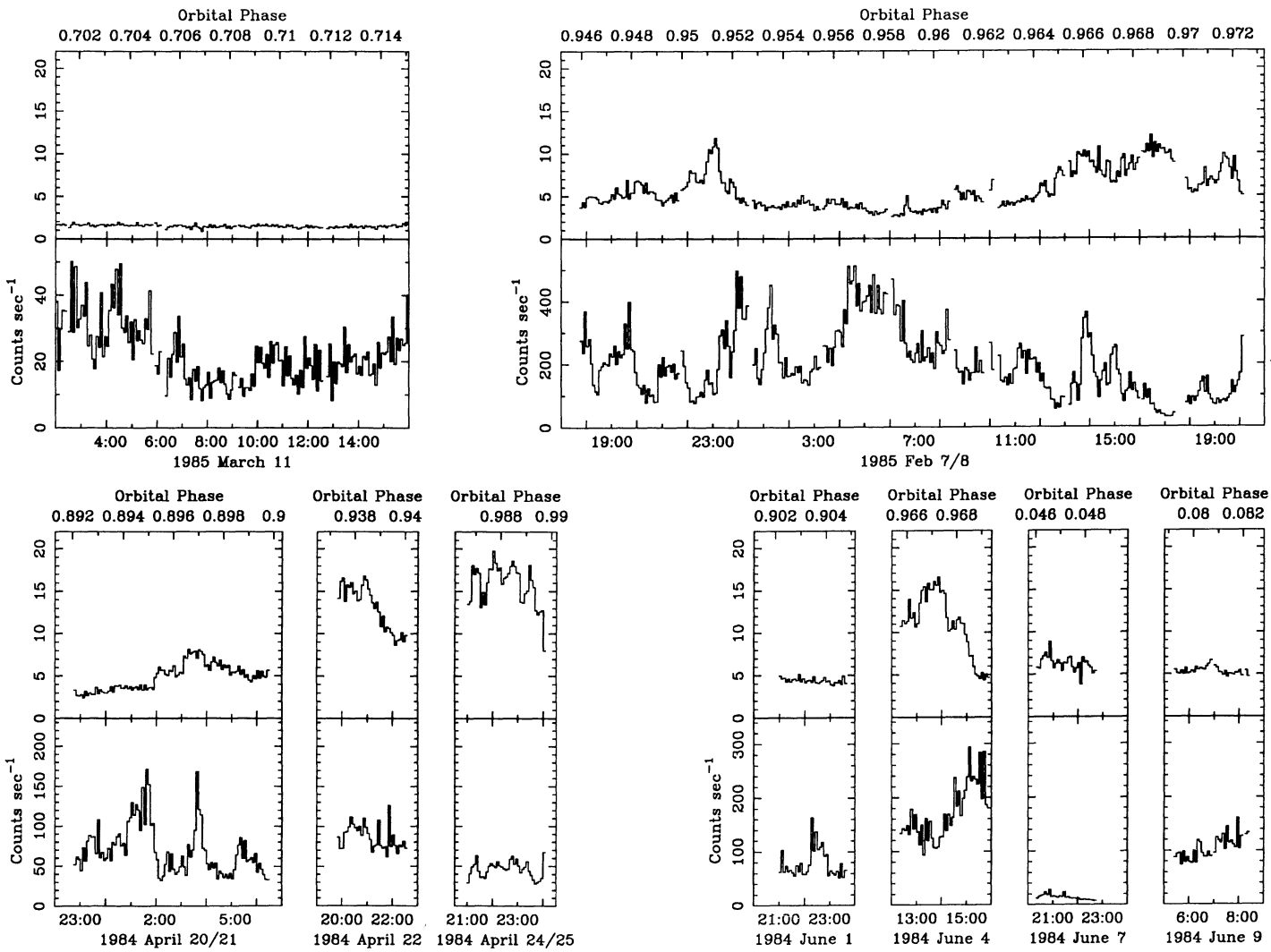

FIG. 1—*Continued*

X-ray properties of GX 301−2 which is discussed in § 6, and in § 7 the conclusions are summarized.

2. OBSERVATIONS

EXOSAT made a total of 13 observations of GX 301−2 each lasting between 3 hr and 2 days (Table 1). Two sets of observations were made in 1984 April (three observations) and in 1984 June (four observations) around periastron passage of the neutron star to monitor the X-ray outburst. A third set of five observations in 1985 February/March was distributed around a single binary orbit to monitor the entire orbital light curve. A detailed description of the *EXOSAT* observatory and its instrumentation can be found in White & Peacock (1988). For this study the medium energy proportional counter array ME, sensitive in the 1–20 keV band, and the gas scintillation proportional counter, GSPC, sensitive in the 2–15 keV band were used. To monitor the particle background, one half of the ME array was offset by $\sim 2°$ excluding the source from the square field of view of 0°.75 × 0°.75 FWHM on each side. The GSPC has a factor of 5 smaller effective area as one half of the ME array, but a factor of 2 better energy resolution.

Aspect-corrected and background-subtracted light curves, obtained by the ME in the 0.9–21.0 keV band, from the three observation sets are shown in Figure 1 with a time resolution of 300 s. A hardness ratio obtained from the ratio of the 5–21 keV to the 0.9–5 keV intensity is shown on the same scale for all observations. The observations within each set are plotted in order of orbital phase coverage. Orbital phases (ϕ) were computed using an orbital period of 41.508 days and a time of periastron passage ($\phi = 0$) of JD 2,443,906.56 (Sato et al. 1986).

During the five observations made in 1985 February/March the overall X-ray intensity in the 0.9–21.0 keV band increased from a minimum of ~ 5 counts s^{-1} at phase 0.15 to about 25 counts s^{-1} at phase 0.7, accompanied by a decrease in hardness ratio from ~ 5 to a minimum of ~ 1.5. The observation around phase 0.96 and the observations from the other sets between phase 0.89 and 0.08 are characterized by strong flaring activity with intensity increases up to 600 counts s^{-1}. During these outburst observations the hardness ratio is highly variable and ranges between 3 and 20.

3. THE SPECTRA

3.1. *The Continuum*

The ME spectra were accumulated in either 64 or 128 PHA channels with a time resolution of 1 and 10 s, respectively

(Table 1) by the *EXOSAT* on-board computer. For the analysis the spectra have been summed into time intervals of between 700 s (the pulsar period) and 3 hr (at $\phi \sim 0.15$), depending on source intensity to give a comparable signal-to-noise ratio in all cases. For the background, spectra from the same detectors were used, offset from the source during nearby time intervals. The spectra were fit to a power-law model with energy index α attenuated by neutral absorption. The only spectra which give an acceptable fit with this model are those from 1985 March 11 ($\phi \sim 0.7$), when the absorption is a minimum. All the other spectra show a low-energy excess below ~ 5 keV. This excess, which has been reported earlier by White & Swank (1984), is similar to that found for 4U 1700−37 (HWK) and Vela X-1 (HW) and accordingly the scattering model which reproduces the spectra from 4U 1700−37 and Vela X-1 was also adopted for GX 301−2.

The scattering model consists of an absorbing medium that passes in front of the X-ray source, with a fraction of the emission scattered to the observer by the ambient stellar wind. The scattered component is absorbed by a lower column density and causes the low-energy excess in a simple absorption model. The power-law energy index could not be well-determined for the GX 301−2 spectra which show a very high absorption, due to an interdependence of α with column density. To constrain α a high-quality ME spectrum was accumulated over the whole observation on 1985 March 11 ($\phi = 0.7$) where the absorption was the minimum and the simple absorption model was sufficient. The spectral fit using this model with a single power-law component gives α of 0.4 and a column density of 9.3×10^{22} H cm^{-2}. To be consistent in using the same spectral model for all observations the parallel absorption model was also used for this spectrum, but the low absorption component was fixed at 5% of the high absorption component and the same power-law index was used for both components. The best-fit gives an energy index of 0.55 for the power law and a column density $N_{\rm H}^{l}$ of 1×10^{22} H cm^{-2} for the low $N_{\rm H}$ component and a column density, $N_{\rm H}^{h}$, of 1.2×10^{23} H cm^{-2} for the high $N_{\rm H}$ component. For all the other observations the power law had a fixed index of 0.55.

Figure 2 shows typical fits to the spectra at various orbital phases using the scattering model. For each model the low and high absorption components are plotted. An iron K emission line near 6.4 keV is included in the fits and is discussed in detail in the following subsection. The residuals are shown below each spectrum. The spectral fits show that the variations in hardness ratio with orbital phase are caused by changes in absorption. The spectrum from 1984 June 7 from an early orbital phase ($\phi = 0.046$) shows high absorption. The absorption decreased on 1985 February 27 at orbital phase $\phi = 0.41$ and reached a minimum during the observation on 1985

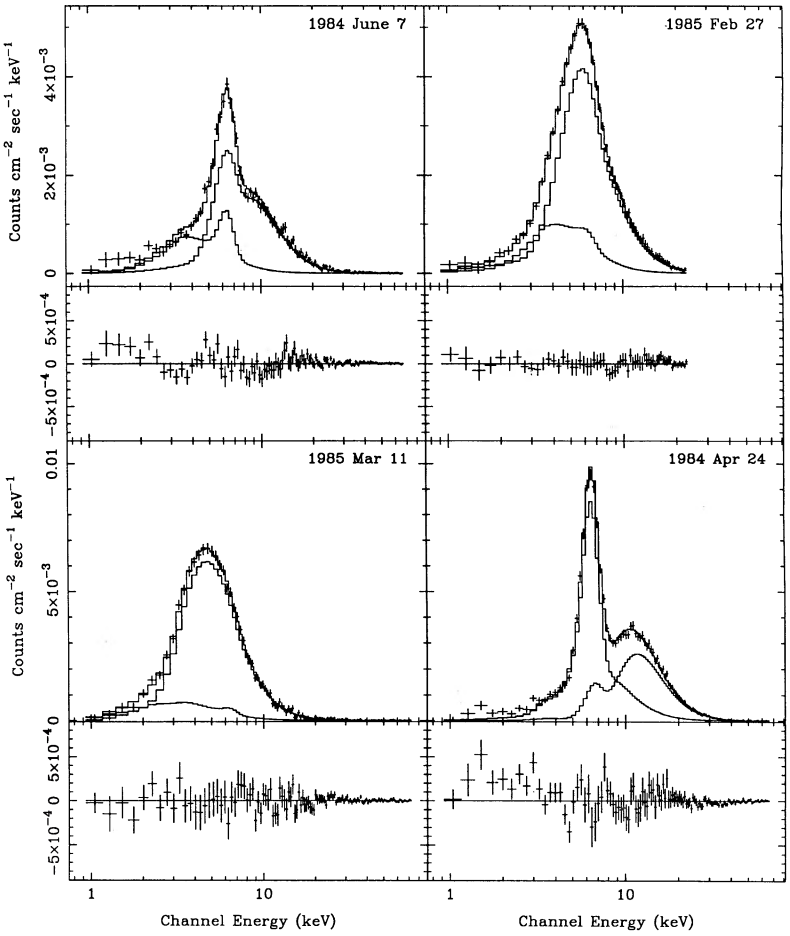

FIG. 2.—Four typical ME spectra from different orbital phases. The best-fitting parallel absorption model is shown for each spectrum together with the two individual components as histograms. The iron line at 6.4 keV is included in the low $N_{\rm H}$ component. Below each spectrum the residuals from the model are shown.

March 11 ($\phi = 0.70$). Around periastron passage of the neutron star between $\phi = 0.89$ and 0.08 the absorption was highest (e.g., 1984 April 24; $\phi \sim 0.99$). The spectra around periastron show the strongest low-energy excess with up to 50% of the high N_H component and the strongest iron K line. The χ_r^2 for the 4 spectra is 1.6, 0.7, 1.0, and 1.5, respectively.

The spectra around periastron when the X-ray source was in outburst do not always give acceptable fits with the scattering model. As can be seen from the residuals of the spectra in Figure 2 from 1984 June 7 and 1984 April 24, the fit is not acceptable at energies below about 3 keV. This spectral behavior, also seen in spectra from 4U 1700−37 during flare maxima (HWK) suggests ionization of the wind by the X-ray source as origin for this additional low-energy excess. X-ray ionization will modify the absorption cross sections (Krolik & Kallman 1984) depending on the distance to the X-ray source. The degree of ionization can be expressed by the dimensionless parameter $\xi = L_x/nr_x^2$, where L_x is the X-ray luminosity, n is the local wind density and r_x is the distance to the X-ray source (Tarter, Tucker, & Salpeter 1969). The ionization decreases gradually with distance to the X-ray source and was approximated with a two-zone model consisting of two media in series, one with opacities for a photoionized gas and one with neutral opacities. This model was introduced by HWK to fit flare spectra from 4U 1700−37 and spectra from Vela X-1 (HW). The spectra give the best fits, when the two-zone model is applied to both, low and high absorption components, although the ionized column density needed to be fixed to the same value used for both components.

Figure 3 shows the column densities of the high absorption component as a function of orbital phase derived from fitting the parallel absorption model and the two-zone model where required to the higher time resolution ME spectra. The neutral column density is plotted in the top panel and decreases from $\sim 1 \times 10^{24}$ H cm^{-2} after periastron passage to a minimum of $\sim 1.2 \times 10^{23}$ H cm^{-2} at phase 0.7. During outburst the two-zone model is required and the ionized column density is plotted in the middle panel. The neutral N_H reaches values up to 1.8×10^{24} H cm^{-2} and the ionized column density is typically 50% of the neutral column density. The ionization parameter ξ was a free parameter in the fits to the spectra and is on average $10^{1.60}$, although some scatter between $10^{1.40}$ and $10^{2.40}$ is seen. The lower panel shows the total direct column density, i.e., the sum of neutral and ionized column density. Figure 4 shows the column densities corresponding to Figure 3 for the low N_H component. This component shows apart from the outburst observations less variations in column density with orbital phase.

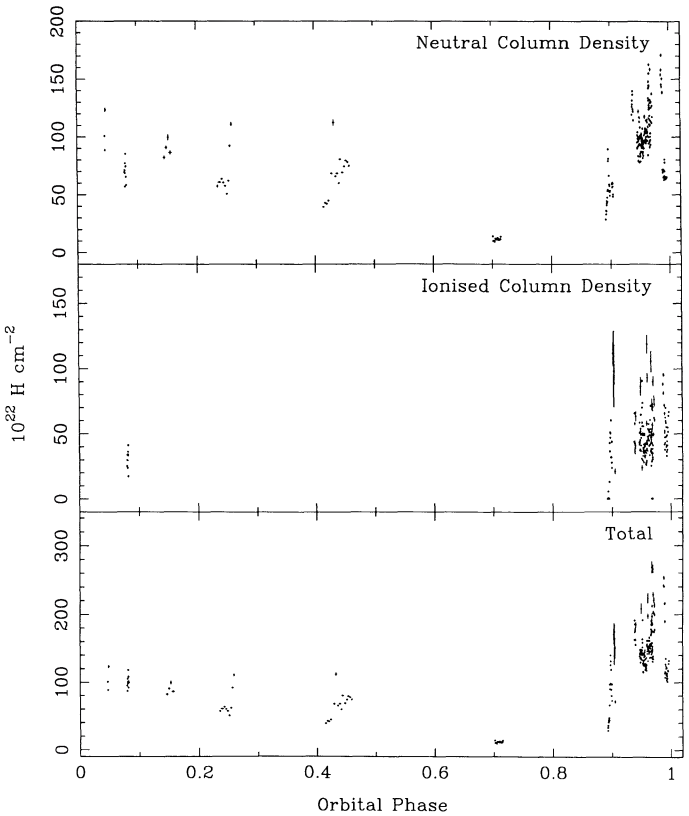

FIG. 3.—Upper panel shows the column density of the direct highly absorbed component derived from fitting the parallel absorption model to the ME spectra as a function of orbital phase. The spectra during outburst and during one observation near phase 0.1 require absorption by ionized gas and the column density for the ionized material is plotted in the middle panel. The total column density along the line of sight, i.e., the sum of ionized and neutral column density is shown in the lower panel.

3.2. *The Iron Line*

A narrow line emission line is seen in the spectra obtained from the GSPC and ME detectors. The energy of the line determined from GSPC spectra was between 6.38 ± 0.07 and 6.54 ± 0.13 keV and is consistent within the errors with that of neutral iron, i.e., 6.4 keV. In the spectral fits to the ME spectra the line energy was a free parameter for the outburst spectra, but away from outburst the counting statistics are lower and the line energy was simply fixed at 6.4 keV. All spectral fits use a line FWHM of 0.1 keV.

In Figure 5 the total unabsorbed flux in the 1–20 keV band is shown in the top panel. The outburst peaks near phase 0.95 with a factor of ~ 100 higher intensity compared to the minimal intensities near phases 0.15 and 0.7. Between the two observations with lowest intensity the intensity is about a factor of 5 higher. In the scattering model the line can be attached to either the low or the high absorption component. The middle panel shows the unabsorbed line intensity as derived adding a line to the low absorption component. The line-equivalent width using the total continuum (low plus high absorption component) is shown in the lower panel. The line intensity follows the variations of the total flux and the resulting equivalent width is more or less constant although there is a considerable scatter for each spectrum. Overall the equivalent width does not exceed 200 eV at any orbital phase. The unabsorbed line intensity as a function of the total flux (low and high absorption component) in the 7–20 keV band is shown in Figure 6*a* with the line added to the low absorption component. By integrating over the continuum above the Fe K-edge energy of 7.1 keV with and without the edge and subtracting the two and with a fluorescence yield of 0.34 the expected fluorescent line intensity can be compared with the observations for different depths of the edge, i.e., different iron column densities. The two solid lines in Figure 6*a* show the expected line intensities for a power-law continuum spectrum with index 0.55 for two values of iron column density which correspond to an equivalent hydrogen column density of 2×10^{22} H cm^{-2} (*lower line*) and 2×10^{23} H cm^{-2} (*upper line*) for cosmic element abundance. The neutral H equivalent column density derived from the spectral fits for the low

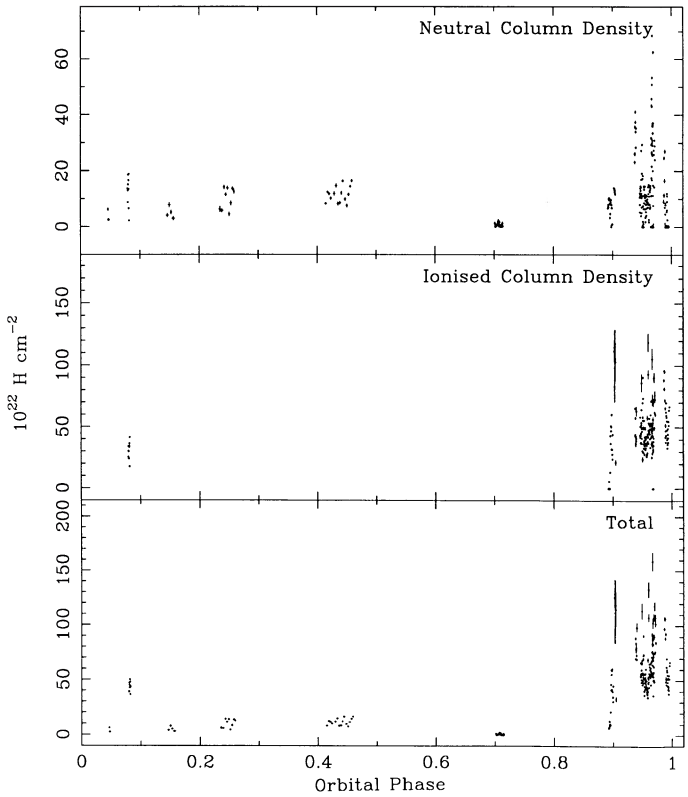

FIG. 4.—Same as Fig. 3, the column density of the low N_H parallel absorption component vs. orbital phase. In the two-zone-model, the ionized column density was fixed at the value of the high N_H component.

absorption component of the ME spectra (see Fig. 4) lies with some exceptions during outburst between 2×10^{22} H cm^{-2} and 2×10^{23} H cm^{-2} and is consistent with the corresponding iron column density. In Figure 6*b* the same is shown for the line added to the high absorption component. The line intensity shows more scatter as in Figure 6*a*. The two solid lines in Figure 6*b* show the expected line intensities for iron column densities corresponding to an equivalent hydrogen column density of 1×10^{23} H cm^{-2} (*lower line*) and 1×10^{24} H cm^{-2} (*upper line*). The first value for the hydrogen column density is the lower limit of the column density derived from the spectral fits for the line added to the high absorption component. More points in Figure 6*b* lie below the lower line as compared to Figure 6*a* which can be explained either by a lower Fe abundance in the material responsible for the fluorescence or that the H equivalent column density of the fluorescing material is overestimated.

4. THE ENERGY DEPENDENCE OF THE PULSE

The analysis of Vela X-1 has shown that the low-energy excess in the X-ray spectra is not pulsed (HW) confirming the scattering model. To study the dependence of the amplitude of the X-ray pulsations on absorption for GX 301−2 the light curves were folded in three energy bands from 0.9–4.9 keV, 4.9–10.0 keV, and 10.0–21.0 keV. Because of the stronger low-energy excess in GX 301−2 spectra, the lower energy band was extended to higher energies as compared to Vela X-1. Figure 7*a* shows the pulse profile on 1985 March 11 when the overall absorption was lowest. The pulse amplitude is normalized to the average counting rate. The pulse profile is in all bands structured as reported in the past (see White, Swank, & Holt 1983). In Figure 7*b* the pulse profile from 1984 February 16 ($\phi \sim 0.15$) is shown, when the absorption was at a very high level and the X-ray intensity was comparable to the 1985 March 11 observation. The pulse profile from Figure 7*b* in the 10–21 keV band shows similar modulations as the corresponding profile in Figure 7*a*. In the 4.9–10 keV band the amplitude is reduced, and in the 0.9 keV band little pulsations are visible with an upper limit for the pulsed fraction of 19% (90% confidence) compared to about 65% in the 10–21 keV band. In the low-energy band the direct high N_H component is completely absorbed and only the low N_H component contributes. A similar behavior is indicated during the outburst observations when the absorption is highest, but an additional dependence of the pulse amplitude on X-ray intensity complicates the pulse profiles of those observations.

5. A STELLAR WIND MODEL

Assuming that the X-rays are powered by material captured from the stellar wind by the neutron star, the X-ray luminosity and absorption properties of GX 301−2 can be used to investigate the density structure of the stellar wind from Wray 977. GX 301−2 is well-suited to derive the wind structure in the radial, azimuthal and polar dimension because the high eccentricity of the system means the neutron star moves through wind with different density as the distance to the primary changes. In addition the line of sight to the neutron star passes through wind above the orbital plane because of the system inclination of around 75°.

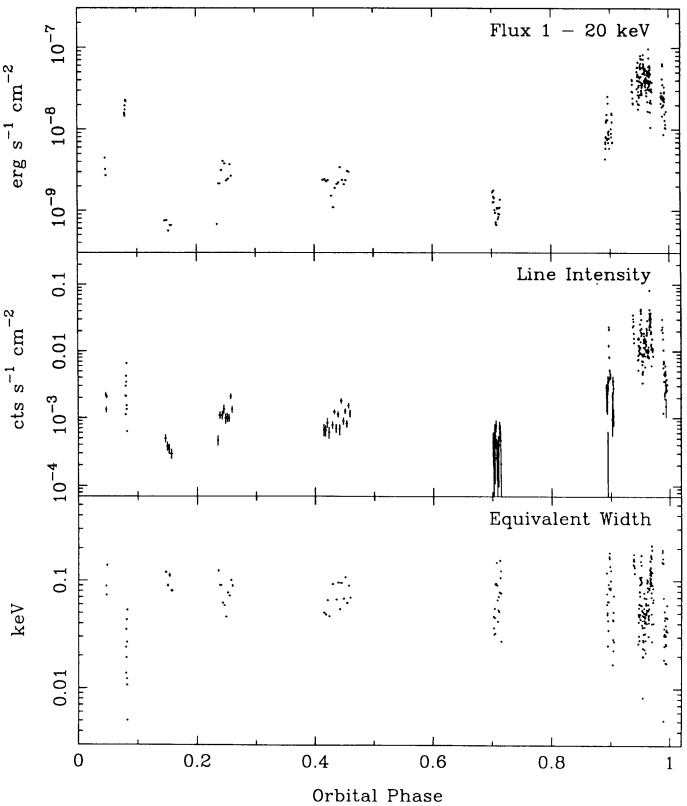

FIG. 5.—Unabsorbed flux, the iron fluorescence line intensity and the line equivalent width from GX 301−2 as function of orbital phase. The iron line is added to the low N_H component of the parallel absorption model. The line equivalent width is calculated using the total continuum, i.e., the sum of the low and high N_H component.

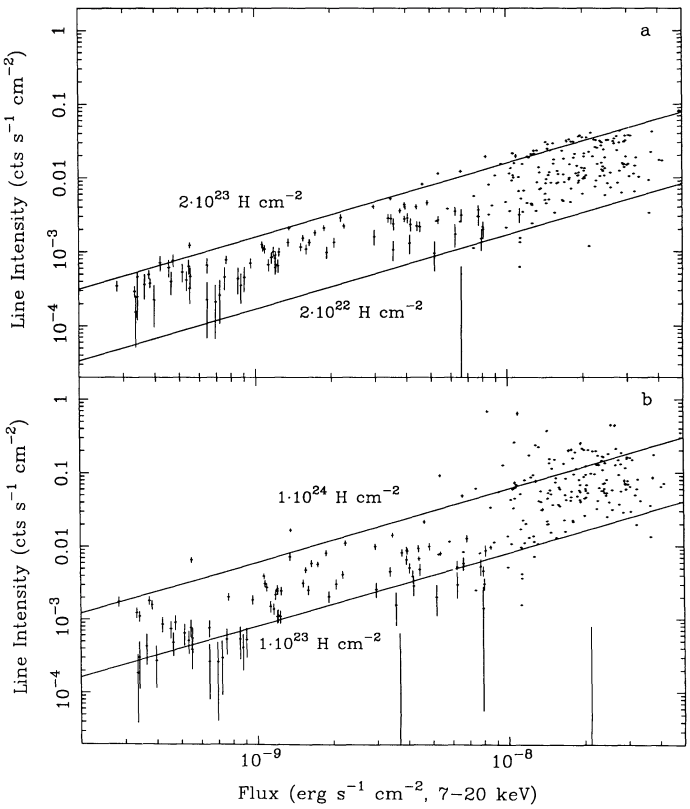

FIG. 6.—Unabsorbed iron line intensity as a function of the total continuum flux in the 7–20 keV band. In (*a*) the line is added to the low absorption component and in (*b*) to the high absorption component. The solid lines indicate the expected line intensities for a fluorescent line with yield 0.34 for different equivalent H column densities.

EXOSAT observations of other SXRBs have shown that the well-known increased absorption at phases after superior conjunction can be explained by a gas stream of enhanced wind density originating at the stellar surface of the primary, trailing the X-ray source. For GX 301−2 a spherically symmetric wind only gives a peak in X-ray absorption around phase 0.25 when we observe the neutron star through the wind very close to the primary (i.e., when X-ray eclipse would occur for a system inclination of 90°). The strong increase in $N_{\rm H}$ after phase 0.9 which continues to stay at high values after periastron passage until phase 0.25 is very similar to the absorption profile of 4U 1700−37 where the strong increase in absorption at phase 0.6 continues to eclipse ingress (HWK). In the following it will be investigated if a model including a gas stream can also reproduce the orbital dependence of the X-ray absorption and X-ray intensity of GX 301−2.

According to Stevens (1988) the neutron star causes enhanced mass loss on the surface of the primary star towards the neutron star. As the neutron star moves further in its orbit, the part of the stellar surface with enhanced mass loss follows the neutron star along the primary equator, leaving behind a region of enhanced density in the wind which will propagate through the wind, forming a gas stream with spiral shape. The curvature of the spiral at a certain distance depends on the radial and rotational velocity of the wind. In modeling the radial wind structure HWK is followed and here only the basic assumptions are given. For the radial velocity the Castor, Abbott, & Klein (1975) law of the form

$$v_w = v_\infty(1 - R_*/r_*)^\alpha \qquad (1)$$

is adopted for the whole wind, including the region of enhanced density. The parameter v_∞ denotes the terminal velocity of the wind, R_* is the radius of the star, and r_* is the distance from the stars center. The parameter α describes the velocity gradient of the wind. Under the assumption of conservation of angular momentum the rotational velocity of the wind is given by

$$v_{w,\rm rot} = v_{\rm eq}(R_*/r_*)\,, \qquad (2)$$

with $v_{\rm eq}$ the rotational velocity of the primary. Conservation of mass requires

$$\rho_w = \dot{M}_*/4\pi r_*^2 v_w\,, \qquad (3)$$

where $\dot{M}_*$ is the mass-loss rate from the primary, and ρ_w is the wind density.

It is assumed that all the material within the capture radius

$$R_c = \frac{2GM_x}{|\boldsymbol{v}_w - \boldsymbol{v}_x|^2} \qquad (4)$$

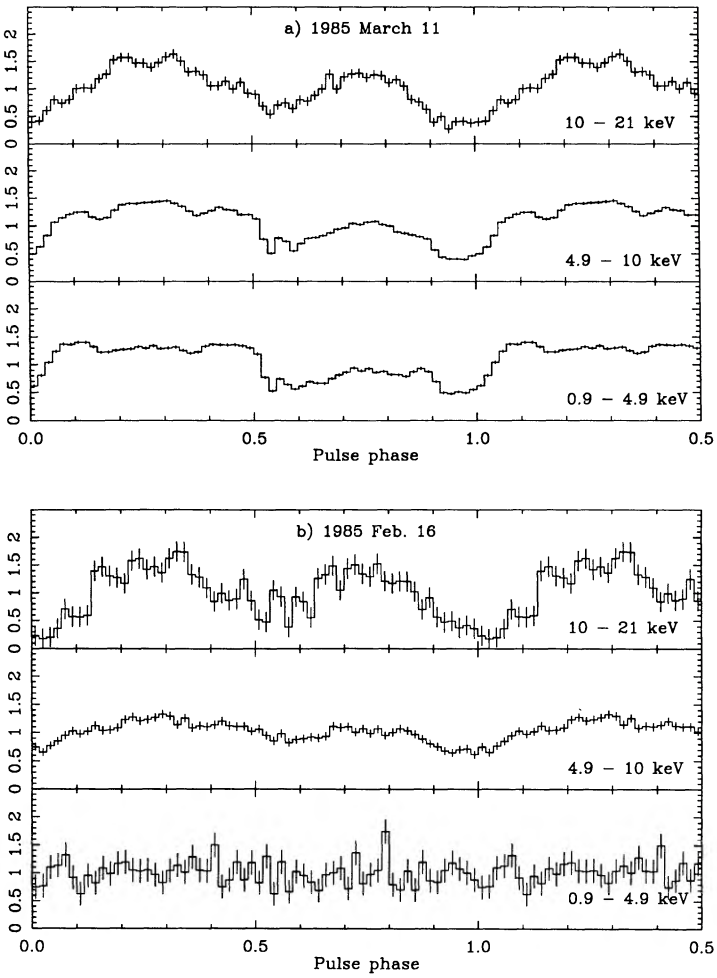

FIG. 7.—Normalized X-ray light curves folded with the pulse period in three different energy bands and plotted vs. an arbitrary pulse phase. During the observation on 1985 March 11 when the absorption was lowest, the pulse profile shows pronounced maxima and minima in all energy bands. The observation on 1985 February 16 showed very high absorption and the pulsations in the lower energy bands are much reduced.

is accreted by the compact object. M_x is the mass of the neutron star and v_x its orbital velocity. The rate of mass captured is then given by

$$\dot{M}_c = \frac{\dot{M}_* R_c^2}{4r_*^2} . \quad (5)$$

This yields the X-ray luminosity by

$$L_x = \frac{\dot{M}_c G M_x}{R_x} , \quad (6)$$

where R_x is the radius of the neutron star, assuming that all the gravitational energy is converted into X-rays.

The following system parameters are assumed: an eccentricity, e, of 0.472, a period, P, of 41.508 days, a longitude of periastron of $-50°.1$, a binary separation a sin (i) of 159 $R_\odot$ (Sato et al. 1986), a system inclination i of 73°, a primary radius of 43 $R_\odot$, a mass loss rate $\dot{M}_* = 4 \times 10^{-6} M_\odot$ yr^{-1} (Parkes et al. 1980), and a neutron star with a mass of 1.4 $M_\odot$ and a radius of 10 km. The rotation period of the primary was assumed to be the orbital period (Parkes et al. 1980) and for simplicity no effects from photoionization of the wind by the X-ray source are taken into account.

The enhanced mass loss from the primary is approximated by a Gaussian-shaped density profile of the form

$$\rho_w(\phi_a, \phi_p) = \rho_w^0 \left[1 + f_c \exp\left(-\frac{\phi_a^2}{\sigma_a^2} - \frac{\phi_p^2}{\sigma_p^2} \right) \right] , \quad (7)$$

where ϕ_a denotes the azimuth starting from the line joining the centers of the stars and ϕ_p the angle in polar direction. The angular size of the region is given by the 1 σ width σ_a and σ_p in azimuth and polar direction, respectively. The mass-loss rate in the center of the region is a factor of f_c higher than the basic mass loss.

Any mass element which is accreted by the neutron star, at a given orbital phase, left the stellar surface at an earlier phase due to the wind flow time. This time lag determines the angular distance ϕ_a of the starting point of the mass element on the stellar surface to the center of the region of enhanced mass loss. Because it is uncertain if the CAK velocity law is valid very close to the primary star, where the slow wind contributes mostly to the flow time, the flow time of the wind between stellar surface and $r_* = 1.05$ was used as a free parameter. Between $r_* = 1.05$ and the neutron star orbit the time lag was calculated from the wind flow time assuming the CAK wind velocity. The angular distance ϕ_a will be reduced by any rotation of the primary in the same sense as the orbital motion of the neutron star because an accreted mass element left the stellar surface a certain angle behind (opposite to the orbital motion) the line joining the centers of the stars and therefore nearer to the region of enhanced mass loss. Figure 8 shows ϕ_a as a function of orbital phase for $v_\infty = 1500$ km s^{-1}, $\alpha = 0.8$ and a wind flow time inside 1.05 stellar radii of 0.15 the orbital period. For these parameters the total wind flow time to the neutron star orbit is between 0.16 the 0.20 the orbital period, depending on orbital phase. The dashed line shows the angular distance to the region of enhanced mass loss of an accreted mass element when it left the stellar surface for a nonrotating primary. Due to the high eccentricity of the GX 301−2 orbit, the angular velocity of the neutron star changes by a factor of ~7. This causes the maximum of ϕ_a near phase 0.1 and the broad minimum around phase 0.6. The angular shift due to a stellar rotation with the same period as the orbital period is shown as dash-dotted line and is nearly constant due to the decreasing angular velocity and the strongly increasing radial velocity of the wind at the distances the neutron star orbit covers. Most of the angular shift is caused near the primary where the radial wind velocity is low and the angular velocity is high. The total angular distance of the mass element to the region of enhanced mass loss is shown as a solid line in Figure 8. The angular distance ϕ_a goes through zero near phase 0.3 and 0.9, i.e., the accreted wind at these phases originated in the center of the region of enhanced mass loss on the primary surface where the wind density is highest and high X-ray luminosities are expected. In other words, the neutron star moves at these phases through the center of the gas stream. Before phase 0.3, where ϕ_a shows the maximum, the dense wind from the region of enhanced mass loss passes the neutron star far behind it and the X-ray luminosity should be near the values expected from the basic wind without enhanced mass loss.

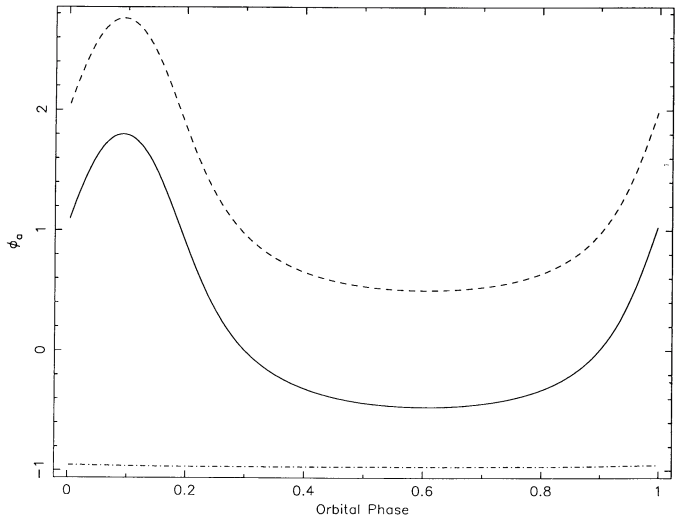

FIG. 8.—Varying angular distance of an accreted mass element in the stellar wind relative to the region of enhanced mass loss when leaving the stellar surface. In this model the neutron star moves twice through the gas stream formed by the enhanced mass loss.

In Figure 9 the model is qualitatively compared with the X-ray luminosity and column density as derived from the spectral fits. The sparse phase coverage and the large scatter of the observed X-ray luminosity and column density do not allow to fit the model to the data. The luminosity from the spectra is calculated in the 1–20 keV band with the absorption set to 0 for a distance of 1.8 kpc. The model uses the same wind parameters as used for Figure 8 and $f_c = 100$, $\sigma_a = 40°$ and $\sigma_p = 20°$. In the lower panel of Figure 9 the column density is shown. The lower solid line describes the contribution of the wind without the gas stream, i.e., for a spherically symmetric wind. It cannot explain the high absorption before phase 0.2 and after 0.9. The upper line includes the gas stream due to enhanced mass loss and the agreement with the data is improved but the model predicts still too little absorption before phase 0.2 and too much absorption around phase 0.7. In the upper panel of Figure 9 the X-ray luminosity is shown. The lower pair of solid lines represents the model without gas stream, the upper pair including the gas stream. The lower line of each pair shows the absorbed luminosity whereas the upper line of each pair the unabsorbed intrinsic luminosity. The strong X-ray outbursts

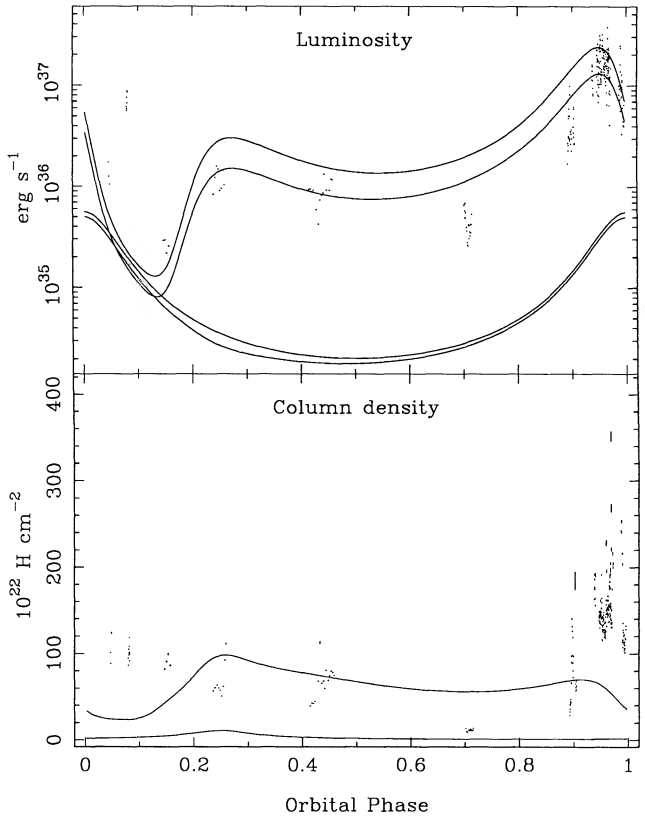

FIG. 9.—Predicted X-ray luminosity and absorption column density for the model with constant mass-loss enhancement. The luminosity from the spectral fits is calculated in the 1–20 keV band with the absorption set to 0 and a distance to GX 301−2 of 1.8 kpc. The lower two lines for the model luminosity indicate the contribution from the wind without the gas stream, the lower of the two with absorption the upper without. The upper two lines represent the total luminosity including accretion from the gas stream, again with and without absorption. The lower line for the column density shows the absorption by the wind without gas stream and in the upper line the contribution of the gas stream is included. The model shows that the gas stream dominates the X-ray properties of GX 301−2.

from GX 301−2 at phase 0.95 can be explained by the pass through the gas stream near periastron.

As for the absorption the model predicts too high X-ray luminosities around orbital phase 0.7. This suggests that the magnitude of the mass-loss enhancement on the stellar surface is lower around apastron as compared to periastron. This was found by Stevens (1988) in his model calculations for A 0538−66 (see, e.g., Fig. 1 of his work). Following this model the maximum mass-loss enhancement factors f_c were calculated as a function of orbital phase from the average ratios of model luminosity and absorption to observed luminosity and absorption respectively. A spline function with knots about phase 0.05 apart was fit to the ratios and the values for f_c at the knots were used for the model. Figure 10 shows f_c after a few iterations as a function of orbital phase. Between the knots the values for f_c were linearly interpolated. In Figure 11 the model with variable mass-loss enhancement is compared with the observed X-ray luminosity and column density as in Figure 9. The agreement with the data is improved for X-ray luminosity and absorption.

6. DISCUSSION

Modeling X-ray luminosity and absorption from GX 301−2 by different authors using spherically symmetric

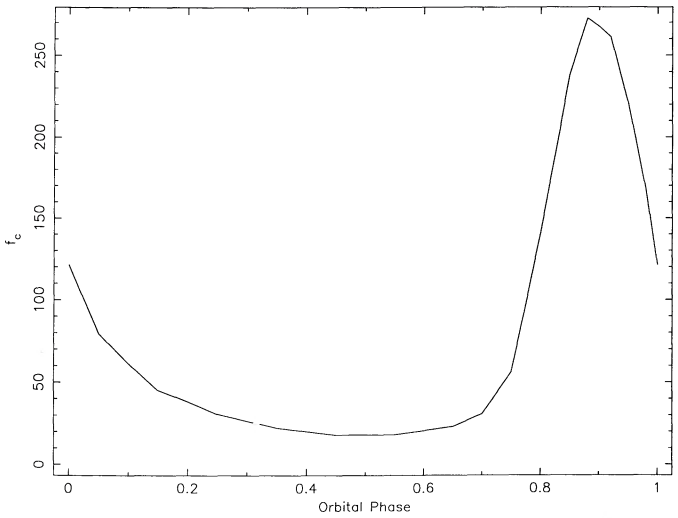

FIG. 10.—Mass-loss enhancement factor f_c as a function of orbital phase calculated from the ratios of observed to model luminosity and column density.

wind flow from the primary has failed to reproduce the X-ray behavior of GX 301−2. The peak luminosity of the X-ray outburst occurs several days before periastron and only implausibly high mass-loss rates of 10^{-4} $M_\odot$ yr^{-1} could reduce the intrinsic luminosity at periastron by absorption due to the dense wind to shift the peak in observed luminosity to earlier phases (Watson et al. 1982). The ratio between peak and minimum luminosity could only be explained by extreme

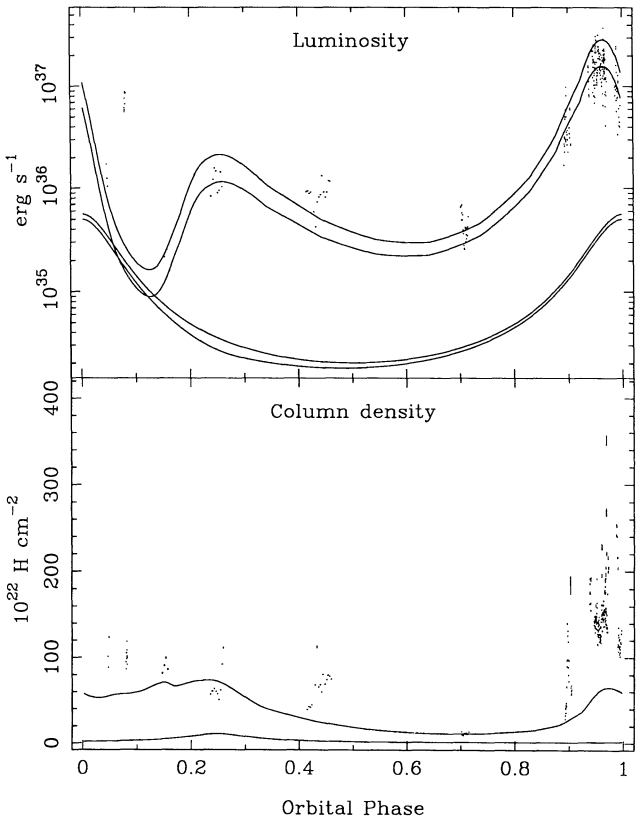

FIG. 11.—Same as Fig. 9, but with the variable mass-loss enhancement factors shown in Fig. 10.

values of mass-loss rate and wind velocity (White & Swank 1984). For a spherically symmetric wind a symmetric X-ray absorption profile is expected around a maximum near phase 0.25 when the X-ray source is observed through the dense wind near the primary (White & Swank 1984). The analysis of the *EXOSAT* data has shown that the column density increases during outburst and stays at a high level until after phase 0.25 with a minimum near phase 0.7.

The X-ray absorption profile of GX 301−2 is similar to that of 4U 1700−37 which could be explained by HWK with a dense gas stream from the primary trailing the X-ray source. A similar gas stream model used in this work can qualitatively reproduce the observed absorption profile of GX 301−2. HWK used a very qualitative model of a radial gas stream for 4U 1700−37 because the circular orbit of 4U 1700−37 does not provide more detailed information about the shape of the gas stream. The eccentric orbit of GX 301−2, however, provides more spatial information about the wind density structure. In this work a gas stream model was used where the gas stream is caused by a region of enhanced mass loss towards the neutron star on the stellar surface of the primary as proposed by Stevens (1988) to explain the X-ray outbursts of recurrent binary X-ray transients with highly eccentric orbits. Due to the variable orbital velocity, the neutron star moves twice through the spiral-shaped gas stream causing the outburst near phase 0.95 and a second broader maximum in X-ray luminosity around orbital phase 0.3 between a deep minimum near phase 0.15 and a weaker minimum around phase 0.7 as observed previously (Rothschild & Soong 1987).

Although the model with constant mass-loss enhancement reproduces already the basic X-ray luminosity properties of GX 301−2, a model with variable mass-loss enhancement improves the agreement with the data, especially the column density. A factor of about 5 higher enhancement f_c around periastron compared to apastron reproduces the observed X-ray luminosity and column density near phase 0.7. Stevens (1988) found in his model for A 0538−66 much higher factors of up to 200. On the other hand the extension for the region of enhanced mass loss of 40° in azimuthal and 20° in polar direction found for GX 301−2 is larger than the $\sim 10°$ found by Stevens for A 0538−66. This might indicate that the properties of the enhanced mass-loss region strongly depend on the eccentricity of the binary system. The elongation of the enhanced mass-loss region in the azimuthal direction might be the result of the changing angular velocity of the orbital motion of the neutron star in the frame of the rotating primary. Absolute values for f_c cannot be determined because they act like the basic mass-loss rate and the terminal wind velocity as normalization factors to column density and X-ray luminosity and are interdependent with those two parameters.

The mass-loss enhancement f_c as a function of orbital phase found for GX 301−2 shows high values near phase 0.9 and is asymmetric around phase 0 in contradiction to the model of Stevens (1988) which gives symmetric values around periastron. The high values around phase 0.9 are caused by the high column density observed between phase 0.9 and 0.2 and barely influence the luminosity as the angular distance of the gas stream is very large at those phases and the neutron star accretes little material from the gas stream. The high column density can also be the result of other effects and the high f_c values near phase 0.9 artificial. A higher rotation rate of the primary increases strongly the column density between phases 0.9 and 0.2 because the spiral-shaped gas stream will be bent more towards the line of sight near the primary. Pakull (1978) reported a photometric period of the optical star of 22.6 days which is about half the orbital period. Another possibility is a second region of enhanced mass loss above a tidal bulge on the primary surface. The lag of a tidal bulge is proportional to the angular velocity of the neutron star in the frame of the rotation primary (Alexander 1973). Due to the changing orbital velocity of the neutron star the position of the tidal bulge changes relative to the line joining the centers of the two stars. If the high f_c values around phase 0.9 are caused by enhanced mass loss above a tidal bulge, then this mass loss would be dominant because of the higher f_c values around phase 0.9 compared to periastron.

The spectra during phases of high absorption when we look through the gas stream show a strong low-energy excess as was also seen from 4U 1700−37 (HWK) and Vela X-1 (HW). The X-ray pulsations in the low-energy excess in the GX 301−2 spectra are greatly reduced which was also seen from Vela X-1 (HW) and confirm the model of X-ray emission scattered by the less dense ambient wind around the gas stream. Around phase 0.95 the column density derived from the spectra shows large variations with increases up to 3×10^{24} H cm^{-2}. This behavior is similar to Vela X-1, where erratic increases in N_H have been reported by Sato et al. (1986) from *Tenma* data and by HW from *EXOSAT* data. HW suggested that the erratic variations in absorption may indicate the formation of a tenuous accretion disk, and may also be occurring in GX 301−2 when the neutron star passes through the gas stream near periastron.

During outburst the spectra show the effects of X-ray ionization on the wind. This was modeled using the two-zone model introduced to HWK to fit a low-energy excess seen in flare spectra of 4U 1700−37. The spectra outside outburst when the X-ray luminosity was about two orders of magnitude lower than during outburst maximum do not show any ionization effect. The large range in X-ray luminosity covered by the spectra from GX 301−2 shows as in the case of the flares from 4U 1700−37 the correlation of the ionization effects with X-ray luminiosity. The average ionization parameter of $10^{1.6}$ is consistent with the values found for Vela X-1 ($10^{1.65}$) and 4U 1700−37 ($10^{1.6}$).

7. CONCLUSIONS

The results from the *EXOSAT* observations of GX 301−2 have demonstrated that the X-ray properties are dominated by a gas stream from the primary Wray 977. The model with enhanced mass loss towards the neutron star forming a spiral-shaped gas stream can reproduce the orbital phase dependence of the X-ray absorption and X-ray luminosity. The X-ray spectra are highly absorbed when the line of sight to the X-ray source passes through the gas stream and show a less absorbed low-energy component. This component can be explained by X-rays scattered around the gas stream by the less dense ambient stellar wind which is confirmed by the nonpulsating nature of the low-energy X-rays. GX 301−2 is, together with 4U 1700−37 and Vela X-1, the third SXRB containing a gas stream. Still uncertain is the origin of the strong flaring activity seen only during the outburst of GX 301−2 and from 4U 1700−37 and might be associated with the distance of the neutron star to the primary.

I thank the other members of the *EXOSAT* Observatory team for their assistance during the observations. In particular I thank Nick White for reading the manuscript and for numerous helpful comments.

REFERENCES

Alexander, M. E. 1973, A&SS, 23, 459
Bradt, H. V., et al. 1977, Nature, 269, 21
Castor, J. I., Abbott, D. C., & Klein, R. I. 1975, ApJ, 195, 157
Haberl, F., & White, N. E. 1990, ApJ, 361, 225 (HW)
Haberl, F., White, N. E., & Kallman, T. 1989, ApJ, 343, 409 (HWK)
Joss, P. C., & Rappaport, S. 1984, ARA&A, 22, 537
Krolik, J. H., & Kallman, T. R. 1984, ApJ, 286, 366
Leahy, D. A., Nakajo, M., Matsuoka, M., Kawai, N., Koyama, K., & Makino, F. 1988, PASJ, 40, 197
Pakull, M. 1978, IAU Circ., No. 3317
Parkes, G. E., Mason, K. O., Murdin, P. G., & Culhane, J. L. 1980, MNRAS, 191, 547
Rothschild, R. E., & Soong, Y. 1987, ApJ, 315, 154
Sato, N., Nagase, F., Kawai, N., Kelley, R. L., Rappaport, S., & White, N. E. 1986, ApJ, 304, 241
Stevens, I. R. 1988, MNRAS, 232, 199
Tarter, C. B., Tucker, W. H., & Salpeter, E. E. 1969, ApJ, 156, 943
Watson, M. G., Warwick, R. S., & Corbet, R. H. D. 1982, MNRAS, 199, 915
White, N. E., & Peacock, A. 1988, Mem. Soc. Astr. Italiana, 59, 7
White, N. E., & Swank, J. H. 1984, ApJ, 287, 856
White, N. E., Swank, J. H., & Holt, S. S. 1983, ApJ, 270, 711